

### Malaysian Journal of Mathematical Sciences

Journal homepage: https://mjms.upm.edu.my



# Effect of Melting Heat and Activation Energy on MHD Williamson Fluid Flow Over Parabolic and Plane Surfaces: A Numerical Approach

Padma Devi, M.\* <sup>1</sup> Ankamma Rao, M. <sup>1</sup> Krishnaveni, B. <sup>1</sup> Sombabu, A. <sup>1</sup> Ankamma Reddy, G. V. <sup>1</sup>

> E-mail: padmadevimedisetti@gmail.com \*Corresponding author

> > Received: 2 December 2024 Accepted: 2 March 2025

### **Abstract**

The complex relationship between fluid motion and curved surfaces significantly affects flow dynamics, yielding intricate patterns and phenomena. Fluid flow over curved geometries, specifically on parabolic geometries, is a crucial phenomenon in multiple engineering disciplines. Parabolic surfaces, characterized by their continuous curvature, are ubiquitous in nature and industrial applications, ranging from aerodynamic wing designs to hydroelectric power plants and biomedical devices. This study delineates the complex interactions among several critical factors like activation energy and melting heat accounting for supplementary factors such as mixed convection, heat source and Cattaneo-Christov formulation. The primary goal of this research paper is to investigate the combined effects of melting heat, activation energy, and magnetic fields (MHD) on the flow, heat transfer, and mass transfer characteristics of a Williamson non-Newtonian fluid over parabolic and plane surfaces. Solutions are derived numerically by employing Matlab's built-in bvp4c function and illustrated graphically for parabolic and plane geometries. Validation exercises reveal a high degree of consistency between numerical results and published data. Parabolic flow exhibits a rapid temperature escalation compared to plane flow. Parabolic flow demonstrates a pronounced concentration drop than in plane flow. A novel comparative scrutiny is carried out on parabolic and plane surfaces in the context of Williamson fluid. This study delineates the complex interactions among several critical factors like activation energy and melting heat, This research seeks to advance understanding in applications such as materials processing, polymer manufacturing, and energy systems. It is evinced that the parabolic surface demonstrates superior skin friction and heat transmission accompanied by reduced mass transport compared to plane surfaces.

Keywords: magnetohydrodynamic; heat source; Cattaneo-Christov formulation; bvp4c.

### 1 Introduction

Non-Newtonian fluids have an important significance in modern engineering. Examples are environmental engineering [47], biological gels [25], polymer processing [36], and energy generation [57]. Non-Newtonian fluids are important in engineering and industrial processes, hence researchers are investigating mass and heat transfer phenomena. Shampoos, jelly, sugar, honey, human blood, pulps, and other products are examples of non-Newtonian fluids. Non-Newtonian fluids' viscosity is typically influenced by shear rate. Non-Newtonian fluids can exhibit stress changes and other non-Newtonian phenomena despite having independent viscosity and shear. The Williamson liquid is a Non-Newtonian and time-invariant liquid with pseudo-plastic traits. Williamson liquid model imparts mathematical framework for the comprehension of pseudoplastic rheology of diverse materials. Pseudoplastic fluids are widely encountered in the manufacture of emulsion-based imaging films, polymeric sheets, transmission of plasma and etc. The Williamson fluid is a model of pseudoplastic fluid. Pseudo-plastic fluids are used in engineering and industry for food processing, blood cells, photographic films, and inkjet printing.

Nadeem et al. [41] performed a comprehensive research on the flow dynamics of Williamson fluid driven by an extending surface. They spotted a parabolic deceleration in skin friction for an escalation in the Williamson term and manifested that Williamson model effectively characterizes the flow features of pseudoplastic liquids. Shafiq and Sindhu [50], employed the effect of hydromagnetics in the Williamson fluid boundary layer flow towards a stretched permeable surface. Human blood flow is an important topic in biomedical research because it can help treat blood diseases. However, experimental research is expensive and time-consuming was studied by Azmi et al. [13]. Shah et al. [51] studied the flow of a Williamson liquid film fluid across a time-dependent stretching surface, including heat transfer and thermal radiation embedded in a porous media.

The combined effects of viscosity, temperature, and slanted Lorentz force on Williamson nanofluid flow across a variable stretching sheet are discussed by Khan et al. [29]. Shawky et al. [53] explored the two-dimensional hydromagnetic flow of an incompressible Williamson nanofluid across a stretched sheet in a porous environment. Kho et al. [33] examined the heat transfer analysis and slip circumstances on a Williamson nanofluid over a stretching sheet. Dada et al. [16] examined the effects of radiation and chemical reactions on heat and mass transport in magnetohydrodynamics (MHD) Williamson fluid flow over a narrowing stretched sheet with varying thickness. The effect of an inclined magnetic field on Williamson fluid on a stretching sheet when convective boundary conditions are present in the nanoparticles was investigated by Srinivasulu and Goud [56]. The research by Reddy et al. [46] approximated a resolution and analyzed the flow attributes of MHD Williamson liquid near a extending cylinder.

Hussain et al. [26] examined the temperature-dependent viscosity and mixed convection affect the flow of SWCNTs and MWCNTs. A comparative analysis of SWCNTs and MWCNTs suspended in base liquid is given. Ali et al. [5] explored the mathematical model to analyse blood flow through a stenosed blood artery. Stenosis illness is characterised by an abnormal constriction of blood flow in the body. A non-Newtonian fluid with yield stress to analyse the complex dynamics of heat transfer in a stagnation-point MHD (Magnetohydrodynamic) convection system was investigated by Anwar et al. [11]. Khan et al. [31] the bioconvective flow of Ree-Eyring across an expanding sheet with a porous media, taking into account the inclined magnetic field and gyrotactic microorganisms. Irfan et al. [28] findings show that the performance of the thermorelaxation factor in the temperature field and the sloutal-relaxation factor in the concentration field is declining. The increasing performance of the mass diffusivity factor has been discovered in the concentration field. Sobhana Babu et al. [55] focusses on how a boundary layer regulates

the movement of a non-Newtonian fluid during a chemical reaction on a radiative paraboloid surface. This involves investigating the fluid's velocity, temperature, and mass transfer. This study focusses on the Williamson fluid model, which is an extended Newtonian fluid.

The automotive industry endeavors to engineer vehicles with reduced frictional or resistive forces. The intricate arrangements found in torpedoes, race cars, aircraft, and spacecraft are of utmost importance in the production of submarines. Likewise, the configuration of munitions, supersonic aircraft, and guided weaponry plays a important role in their manufacture. Because of the hydrodynamics of the system, the streamlines encounter almost no resistance, and the bulk of the contours are excellent approximations to a small set of paraboloid surfaces. The theoretical framework presented by Davis and Werle [17] elucidates the dynamics governing the movement of a Non-compressible, viscous Newtonian fluid across a surface that conforms to the geometric profile of a paraboloid of revolution. Khan et al. [32] explored the dynamic processes of quartic autocatalysis chemical reactions in Williamson nanofluid flow on a parabolic surface to optimise and increase the efficiency of industrial and technical systems with intricate fluid dynamics and chemical reactions.

Analysed are the movements of gyrotactic microorganisms past a paraboloid of revolution (uhspr), a quartic autocatalysis chemical process, and the flow of a Williamson nanofluid with Cattaneo-christov (C–C) heat flux. Animasaun and Sandeep [9] conducted a study to analyse the phenomeNon of buoyancy-induced flow in a nano fluid. The nano fluid was composed of 36nm alumina particles that were dispersed in water. The researchers specifically focused on the behaviour of the nano fluid as it moved over a paraboloid of revolution. In their study, Makinde and Animasaun [37] conducted an investigation on the flow characteristics of a 36nm alumina and water-based nanofluid over a paraboloid of revolution, while taking into account the phenomenon of bioconvection. Koriko et al. [34] introduced a new version of buoyancy-induced flow of 29nm CuO and water-based nano fluid powered of a paraboloid of revolution by an upper surface.

Abegunrin et al. [3] as well as Animasaun et al. [8] conducted a theoretical investigation on the behaviour of fluid over a Non-horizontal, Non-vertical, Non-inclined, Non-wedge, and Noncone surface. Their study incorporated catalytic surface reactions. Khan et al. [32] summarized the flow features of MHD bio convective Newtonian fluid caused by a parabolic revolution with chemical reaction. Santoshi et al. [49] provided a succinct overview of the flow characteristics exhibited by magnetic Carreau/Casson fluids when traversing a porous paraboloid of revolution while being subjected to convective limitations. By taking a variety of factors into consideration, Zeeshan et al. [58] and Gangadhar et al. [23] explored the various physical properties of a pair stress fluid that was created by a parabolic surface in the presence of catalytic surface reactions. Naik et al. [42] investigated various fluid flows through an expanded plate. The effects of viscous dissipation, activation energy, and chemical reaction are considered while modelling the investigated physical events.

Magnetohydrodynamic boundary layers for heat and mass transmission over surfaces are employed in a variety of technical and geophysical applications, including nuclear reactor cooling, packed-bed catalytic reactors, geothermal reservoirs, thermal insulation, and enhanced oil recovery. Recently, elucidating and modeling the intricate behavior of complex fluid flows has emerged as a pivotal research domain. Researchers have shown keen attention in studying the role of extrinsic factors, specifically magnetic fields. Magnetohydrodynamics (MHD) is a scientific field which concerned with the comprehension of features of electrically conductive liquids in the environment of magnetic force. This factor has extensive practical utilizations encompassing liquid transportation, electrical energy production, metal shaping and nuclear fusion technology. MHD is extensively employed because it enables the regulation on fluid motion via electromagnetic forces. Investigating the MHD flow of a Williamson fluid with Dufour and Soret effects is the

aim of the current investigation. The primary focus was examined by Hayat et al. [24], who used a more comprehensive application of modified Darcy's rule to discuss these effects in the presence of permeable medium. The novel part of the current work was examined by Shashikumar et al. [52], who built a Williamson fluid model for thermal analysis of MHD flow along a microchannel in the presence of convective heating and viscous dissipation. The nature of MHD heat and mass transmission was investigated by Kumaran and Sandeep [35]. Theoretical discussion of Williamson and Casson fluids is presented using thermophoresis and the Brownian moment in relation to an upper paraboloid of revolution. Both diffusion-thermo and thermo-diffusion effects are taken into account in the model.

Khan et al. [30] investigated how a magnetic field, thermal resistance, and chemical processes affect the heat and mass transfer parameters of an MHD WNF flowing across a stretched sheet immersed in porous media. Rasheed and Anwar [45] explored the magneto-hydrodynamic flow of viscoelastic liquid using a revised thermal flux model. Ganesh Kumar et al. [22] investigate the flow and thermal properties of a sheet that is continually stretched. Variable thermal conductivity must also be considered while calculating temperature. Furthermore, the flow problem takes into account the convective circumstances of heat and mass transport. Padma Devi et al. [44] studied the computational methods to investigate the unsteady two immiscible MHD free convective flow of Casson liquid along a vertical channel with a porous media. Devi and Srinivas [18] explored the MHD oscillatory flow of two immiscible, viscous liquids in a porous channel with heat transfer.

The pivotal role of activation energy in mass transmission across crucial disciplines like food production, chemical processing, oil emulsions and geothermal energy has garnered substantial attention from the scientists. Arrhenius pioneered the idea of activation energy in 1889. It is the smallest quantity of energy which is essential for particles to engage in a chemical reaction. Reactants must possess activation energy to facilitate their conversion into products. Bestman [14] initially investigated the boundary wall moves in its own plane with suction. This article discusses free convective boundary layer flow in a porous material with simultaneous mass and heat transmission. The paper also covers chemical processes for the simplest model of a binary reaction with Arrhenius activation energy. Makinde et al. [38] studied how energy of activation interacts with chemical reactions (nth-order) in unsteady flow across a flat radiated permeable surface. Alsaadi et al. [6] addressed the entropy generation on the MHD motion of a 2nd grade liquid by incorporating the activation energy across an extending sheet. Their examination divulged that enhancing the activation energy factor yields higher concentrations. Khan et al. [29] explored the thermophysical characteristics of Williamson nanofluid flow across a rotating stretchable surface in magnetohydrodynamics (MHD) while taking activation energy, nonlinear thermal radiation, Joule heating, and changing thermal coefficient into account. Irfan et al. [27] formulated an unsteady model for the flow of Carreau fluid to assess the consequences of activation energy. Their work highlighted that the introduction of the reaction rate term causes alterations in the rheological attributes of Non-Newtonian fluids which yielded lower concentrations.

Nihaal et al. [43] analyzed the Darcy-Fochheimer assisted flow of a ternary fluid driven by an extendable disk and influenced by activation energy. The findings suggest that harnessing bioconvection phenomena can significantly enhance the heat transmission of the base fluid and facilitating more efficient heat transmission. Azhar et al. [12] scrutinized the consequences of activation energy on MHD flow of a ternary fluid around a expandable disk by incorporating variable viscosity. The current communication aimed to investigate the flow properties of carbon nanotubes (CNTs) across a stretching surface, which was accomplished. In addition, the impacts of radiation, chemical processes, and activation energy are studied by Singnaik et.al [54].

Heat transmission is caused by the temperature differential between two dissimilar bodies. It is essential for energy production, cooling nuclear reactors, and biological uses like medication tar-

geting and tissue heat conduction. Transfer of heat was first described by Fourier [20], a parabolic energy equation for temperature field. Its drawback is that the first disruption is detected rapidly across every aspect of medium. Â The Williamson fluid model was used to numerically simulate MHD flow on a variable thickness sheet by Salahuddin et al. [48]. A modified form of Fourier's law, the Cattaneo-Christov heat ux model, is used to study heat transmission phenomena. Cattaneo [15] extended the Fourier law of heat conduction with the thermal relaxation factor. Sluggish thermal waves transport heat when thermal relaxation time is introduced. Mustafa [40] studied the Cattaneo-Christov heat flow model for Maxwell fluid on a stretchable sheet. He discovered that thermal relaxation time and thermal boundary layer thickness are inversely proportional. Current theoretical and computational research within the Darcy-Forchheimer medium using electromagnetic fields has revealed the heat and mass transportation properties of Williamson-Sutterby nanofluid flow under the effects of Cattaneo-Christov double diffusion, radiation heat flux, magnetic dipole, and convective boundary over a stretchy surface.

Ganesh Kumar et al. [21] explored the flow of tangent hyperbolic fluid across a moving stretched surface. The features of heat transmission are provided by using nonlinear radiation. Activation energy characterises other characteristics of mass transfer. The variable thermal conductivity theory also explains heat transport phenomenaMixed convection refers to the combined effects of free and forced convection. It is widely employed in technical applications like as solar collectors, electronics, and nuclear power plants. When buoyancy force dominates the forced convective process, or forced flow dominates the free convective process, such a process occurs, as studied by Dhruvathara et al. [19]. Anwar et al. [10] paper offers a thorough examination of heat transfer and flow dynamics in magnetohydrodynamic (MHD) hybrid nanofluids. Alsa'di et al. [7] investigated the theoretical, analytical, and approximate solutions to the Caputo fractional Volterra-Fredholm integro-differential equations (FVFIDEs).

This study uniquely investigates the Magnetohydrodynamic (MHD) flow of a Williamson fluid over parabolic and plane surfaces, comprehensively comparing these geometries under similar physical conditions. The simultaneous consideration of melting heat and activation energy effects in the flow dynamics introduces a new perspective on thermal and mass transfer phenomena for non-Newtonian fluids. By employing an efficient numerical approach, by using bvp4c solver in MATLAB the study enhances the accuracy of solutions for complex governing equations. The analysis extends the understanding of MHD effects on non-Newtonian Williamson fluid behaviour, particularly in varying thermal and concentration boundary conditions. The findings provide insights into real-world applications such as polymer extrusion, geothermal energy systems, and cooling technologies, where Williamson fluids and MHD effects play a critical role. Existing research focuses on flat or cylindrical surfaces, with minimal attention to parabolic geometries and their unique flow characteristics. While these factors have been studied individually in fluid dynamics, their combined impact on the behaviour of MHD Williamson fluids remains underexplored.

The authors discerned a substantial knowledge scarcity on the collective impression of parabolic surface, activation energy and Cattaneo-Christov on the flow dynamics of Williamson fluid accounting for supplementary factors such as mixed convection, heat source. Despite of extensive research on parabolic surfaces, specifically for Williamson fluids on a parabolic surface within activation energy and melting heat, presents opportunities for future study. Thus, the primary motive and originality of this research is to impart a comprehensive understanding of how activation energy and melting heat affect Williamson fluid flow on a parabolic surface, with particular emphasis on mixed convection and heat source. This research endeavors to impart insight into the multifaceted relationships between various factors affecting fluid flow and elucidate the underlying mechanisms that influence the flow dynamics.

## 2 Physical Questions

Upon concluding our in depth analysis, we have developed the essential insights to address the following vital issues:

- What major repercussions do our findings highlight regarding the complex interconnection between Williamson fluid and liquid velocity?
- In what manner does melting heat alter the liquid temperature?
- In what manner does activation energy alter the liquid concentration?

## 3 Basic Assumptions

The investigation tractable, we employ the following assumptions:

- 1. The fluid is an incompressible Williamson fluid with non-Newtonian viscoelastic properties.
- 2. The flow is considered two-dimensional, steady, and laminar over parabolic and plane surfaces. The surfaces are impermeable, and the fluid flow adheres to the no-slip condition at the surface.
- 3. A uniform magnetic field is applied perpendicular to the flow direction, with no induced magnetic field or Hall effect considered. The magnetic Reynolds number is small, implying that the magnetic field does not vary with the fluid flow.
- 4. Heat transfer is influenced by melting at the surface, which absorbs some thermal energy.
- 5. The Cattaneo-Christov heat flux model (if applied) accounts for finite heat propagation speed (thermal relaxation time).
- 6. Concentration variations are governed by species diffusion and activation energy effects.
- 7. The reaction rate is temperature-dependent and follows an Arrhenius-type exponential relation.

# 4 Model Description

The transport perusal of a steady, 2D and viscous Williamson fluid towards an upper parabolic surface is explored. It is assumed that natural convection is driven by buoyancy. The domain is  $B_1\sqrt{(x+c_1)^{1-m}} \leq y < \infty$ , as shown in Figure 1.

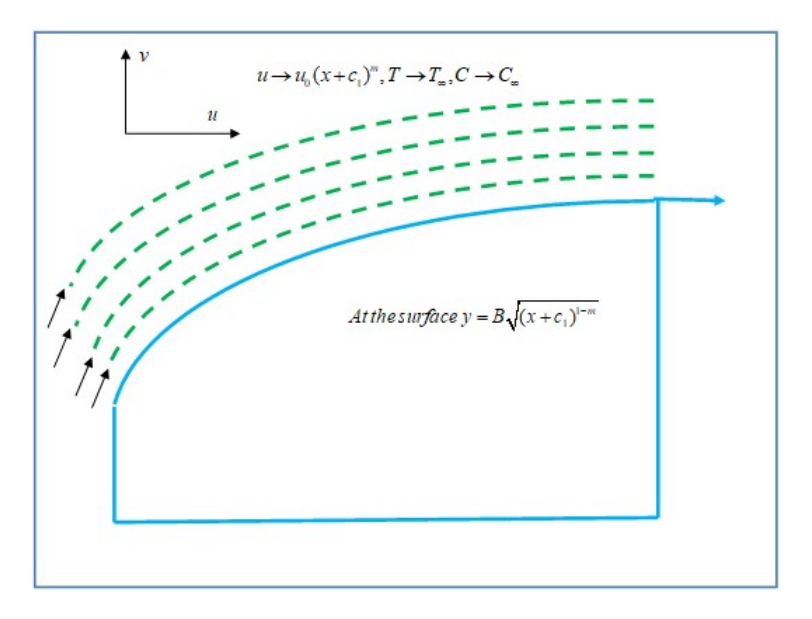


Figure 1: Flow geometry.

Here,  $(m(<1),c_1)$  are power index of velocity and stretching constraint, respectively. The fluid layers on the surface are stretched parallel with velocity  $U_W = U_O(x+c_1)^m$ . The variable magnetic field of strength  $B(x) = B_o \sqrt{(x+c_1)^{m-1}}$  is applied normal to the surface of the parabola. To analyze the heat and mass transport attributes thermal radiation and chemical reaction are incorporated. Hence, with the above specified constraints over a parabolic surface Williamson fluid flow can be modeled as [1,2].

$$(u)_x + (v)_y = 0, (1)$$

$$u u_x + v u_y = \frac{\mu}{\rho} u_{yy} + \frac{2\mu\sqrt{\Gamma}}{\rho} u_y u_{yy} - \frac{\sigma B^2}{\rho} u + g\beta_{X_1} \frac{1+m}{2} (T - T_m) + g\beta_{X_2} \frac{1+m}{2} (C - C_\infty),$$
(2)

$$uT_x + vT_y + \lambda_1 \lambda_1 u^2 T_{xx} + \lambda_1 v^2 T_{yy} + \lambda_1 2uv T_{xy} + \lambda_1 u u_x T_y + \lambda_1 u v_x T_y + \lambda_1 v u_y T_x + \lambda_1 v v_y T_y$$

$$= \frac{k}{\rho c_p} T_{yy} + \tau * \left[ D_B T_y C_y + \frac{D_T}{T_\infty} (T_y)^2 \right] + \frac{Q_X}{\rho c_p} (T - T_m),$$
(3)

$$uC_x + vC_y\lambda_2u^2C_{xx} + v^2C_{yy} + 2uvC_{xy} + uu_xC_x + uv_xC_y + vu_yC_x + vv_yC_y$$

$$= D_B C_{yy} + \frac{D_T}{T_{\infty}} - K_s^2 \left(\frac{T}{T_{\infty}}\right)^s e^{-\frac{E_a}{k_1 T}} (C - C_{\infty}), \tag{4}$$

with the boundary conditions are

$$u - u_w = 0,$$
  $k \frac{\partial T}{\partial y} = \rho v \left( L^* + C_s^* (T_m - T_0) \right),$   $T - T_m = 0,$   $C - C_w = 0,$   
at  $y = B_1 \sqrt{(x + c_1)^{1-m}}$  (5)

$$u \to 0, \quad T \to T_{\infty}, \quad C \to C_{\infty}, \quad \text{as} \quad y \to \infty.$$
 (6)

Here,

(x, y): velocity components,

 $\Gamma$ : Williamson parameter,

g: gravitational constant,

 $c_p$ : specific heat,

 $D_B$ : diffusion constant,

 $\sigma$ : electrical conductivity.

Non-dimensionalization of (2)–(6) can be done by the use of stream function  $u = \psi_y$ ,  $v = -\psi_x$ , along with as [1, 2].

$$\xi = y\sqrt{\frac{1+m}{2}}\frac{u_0}{\vartheta}\left(x+c_1\right)^{m-1}, \quad \psi(\xi) = F(\xi)\sqrt{\frac{2\vartheta u_0}{1+m}}\left(x+c_1\right)^{1+m}, \quad G(\xi) = \frac{T-T_m}{T_\infty-T_m},$$

$$H(\xi) = \frac{C-C_\infty}{C_w-C_\infty}, \quad \beta_{X_1} = \beta_1\left(x+c_1\right)^{2m-1}, \quad \beta_{X_2} = \beta_2\left(x+c_1\right)^{2m-1}, \quad Q_X = Q_o\left(x+c_1\right)^{m-1},$$

$$K_s^2 = k_s^2\left(x+b\right)^{\frac{n-1}{2}}, \quad \lambda_1 = \beta_T\left(x+c_1\right)^{1-m}, \quad \lambda_2 = \beta_C\left(x+c_1\right)^{1-m}, \quad Nb = \frac{\tau D_B\left(C_w-C_\infty\right)}{\vartheta}$$

$$Nt = \frac{\tau D_T\left(T_m-T_\infty\right)}{\vartheta T_\infty}, \quad We = 2\sqrt{\Gamma}u_0\sqrt{\frac{1+m}{2}}\frac{u_0}{\vartheta}\left(x+c_1\right)^{3m-1}, \quad \Pr = \frac{\mu c_p}{k}, \quad Q = \frac{Q_o}{\rho c_p U_o},$$

$$M_h = \frac{c_p(T_\infty-T_m)}{L^*+C_s^*(T_m-T_0)}, \quad Gt = \frac{g\beta_1(T_m-T_\infty)}{U_0^2}, \quad Gs = \frac{g\beta_2(C_w-C_\infty)}{U_0^2}, \quad M = \frac{2}{1+m}\frac{\sigma}{\mu_0}\frac{B_0^2}{\rho}$$

$$Sc = \frac{\vartheta}{D_B}, \quad \sigma = \frac{k_s^2}{U_0}, \quad \delta = \frac{T_m-T_\infty}{T_\infty}, \quad E = \frac{E_a}{k_1T_\infty}, \quad \alpha = B\sqrt{\frac{(1+m)u_0}{2\vartheta}}, \quad \beta_T = \beta_1 U_o,$$

$$\beta_C = \beta_2 U_o.$$

The transformed governing equations are followed as,

$$F'''(\xi) + WeF''(\xi)F'''(\xi) + GtG(\xi) + GsH(\xi) - MF'(\xi) - \frac{2m}{m+1}F'^{2}(\xi) + F(\xi)F''(\xi) = 0, \quad (7)$$

$$G''(\xi) + PrNbG'(\xi)H'(\xi) + PrNtG'(\xi)^{2} + PrF(\xi)G'(\xi)^{2} + Pr\beta_{T}F(\xi)^{\frac{m-3}{2}}F'(\xi)G'(\xi) - Pr\beta_{T}\frac{m+1}{2}F(\xi)^{m}G''(\xi) + PrQG(\xi) = 0,$$
(8)

The transformed boundary conditions are,

$$F(\alpha) = \frac{1-m}{m+1}\alpha,\tag{10}$$

$$F'(\alpha) = 1$$
,  $G(\alpha) = 0$ ,  $H(\alpha) = 1$ , at  $\alpha = 0$ .

$$F'(\alpha) = 0, \quad G(\alpha) = 1, \quad H(\alpha) = 0, \quad \text{at} \quad \alpha \to \infty.$$
 (11)

For Non-dimensionalization of boundary conditions, define the transformations,

$$F(\xi) = F(\eta - \alpha) = f(\alpha),$$
  

$$G(\xi) = G(\eta - \alpha) = g(\alpha),$$

which transmutes the equations and boundary conditions  $[\alpha, \infty) \to [0, \infty)$ . The final equations and boundary conditions can be written as,

$$f'''(\eta) + We f''(\eta)f'''(\eta) + Gt g(\eta) + Gs h(\eta) - Mf'(\eta) - \frac{2m}{m+1}f'^{2}(\eta) + f(\eta)f''(\eta) = 0, \quad (12)$$

$$g''(\eta) + \Pr{Nb \, g'(\eta) h'(\eta)} + \Pr{Nt \, g'(\eta)^2} + \Pr{f(\eta) g'(\eta)} + \Pr{\beta_T \frac{m-3}{2} f(\eta) f'(\eta) g'(\eta)}$$

$$- \Pr{\beta_T \frac{m+1}{2} f''^2(\eta) g''(\eta)} + \Pr{Q \, g(\eta)} = 0,$$
(13)

$$h''(\eta) + \frac{Nt}{Nb}g''(\eta) + Scf(\eta)h'(\eta) + Sc\beta_C \frac{m-3}{2}f(\eta)f'(\eta)h'(\eta) - Sc\beta_C \frac{m+1}{2}f''^2(\eta)h''(\eta) - Sc\frac{2\sigma}{n+1}(1+\delta g(\eta))^s e^{-\frac{E}{1+\delta g(\eta)}}h(\eta) = 0,$$
(14)

subject to dimensional boundary conditions,

$$f(0) = \frac{1-m}{m+1}\alpha, \quad f'(0) = 1, \quad g(0) = 0, \quad h(0) = 1, \tag{15}$$

$$f'(\infty) \to 0, \quad g(\infty) \to 1, \quad h(\infty) \to 0.$$
 (16)

Physical quantities in the flow of Williamson fluid flow which are skin friction coefficient  $Cf_x$ , Nusselt number  $Nu_x$  and Sherwood Number  $Sh_x$  are defined as,

$$Cf_{x} = \frac{\tau_{w}}{\rho u_{w}^{2} \sqrt{\frac{1+m}{2}}} = \frac{\mu u_{y} + 2\sqrt{\Gamma}\mu u_{y}u_{y}}{\rho u_{w}^{2} \sqrt{\frac{1+m}{2}}}, \quad \text{at} \quad y = B\sqrt{(x+c_{1})^{1-m}}, \quad (17)$$

$$Nu_x = \frac{(x+c_1)q_w}{k_o(T_w - T_\infty)} = \frac{-(x+c_1)k_o(1+R)T_y}{k_o(T_w - T_\infty)}, \quad \text{at} \quad y = B\sqrt{(x+c_1)^{1-m}}, \quad (18)$$

$$Sh_{x} = \frac{(x+c_{1})q_{m}}{D_{B}(C_{w}-C_{\infty})} = \frac{-(x+c_{1})D_{B}C_{y}}{D_{B}(C_{w}-C_{\infty})}, \quad \text{at} \quad y = B\sqrt{(x+c_{1})^{1-m}}.$$
 (19)

On simplification we get

$$\sqrt{\text{Re}_x} C f_x = f''(0) \left[ 1 + We \, f''(0) \right],$$

$$\frac{1}{\sqrt{\text{Re}_x}} N u_x = -(1 + R) g'(0),$$

$$\frac{1}{\sqrt{\text{Re}_x}} S h_x = -h'(0).$$
(20)

# 5 Numerical Interpretation

Due to the complexity and nonlinearity of the flow equations governing the proposed model, it is tedious to perceive precise analytical solutions. Thus, the bvp4c solver in MATLAB facilitates the computation of numerical solutions for these complex problems and offers a viable solution strategy for addressing these challenges. The bvp4c differs significantly from earlier techniques since bvp4c eliminates the prerequisite of an initial guess. To initialize bvp4c, the subsequent variables are specified,

$$f(\eta) = f_1, \quad f'(\eta) = f_2, \quad f''(\eta) = f_3, \quad g(\eta) = g_1, \quad g'(\eta) = g_2, \quad h(\eta) = h_1, \quad h'(\eta) = g_2.$$
 (21)

With the help of above variables (12)-(16) can be transfigured as,

$$f'_{3} = \frac{\frac{2m}{m+1}f_{1}^{2} - f_{1}f_{3} + Mf_{2} - Gtg_{1} - Gsh_{1}}{1 + Wef_{3}},$$
(22)

$$g'_{2} = \frac{-\operatorname{Pr}\left(Nb\,g_{2}\,h_{2} + Nt\,g_{2}^{2} + f_{1}\,g_{2} + \beta_{T}\frac{m-3}{2}f_{1}f_{2}g_{2} + Q\,g_{1}\right)}{1 - \beta_{T}\frac{m+1}{2}f_{1}^{2}(\eta)},$$
(23)

$$h'_{2} = \frac{-\frac{Nt}{Nb}g'_{2} - Sc\left(f_{1}h_{2} + \beta_{C}\frac{m-3}{2}f_{1}f_{2}h_{2} - \frac{2\sigma}{n+1}(1+\delta g_{1})^{s}e^{-\frac{E}{1+\delta g_{1}}}h_{1}\right)}{1 - \beta_{C}\frac{m+1}{2}f_{1}^{2}(\eta)},$$
 (24)

subject to,

$$Meg_{2a} + \Pr\left(f_{1a} - \frac{1-m}{m+1}\alpha\right) = 0, \quad f_{2a} = 1, \quad g_{1a} = 0, \quad h_{1a} = 1,$$
 (25)

$$f_{2b} = 0, g_{1b} = 1, h_{1b} = 0.$$
 (26)

### 6 Results and Discussion

This section visually illustrates the consequences of newly identified parameters on associated flow patterns via graphs, supplemented by tabular data highlighting their impact on key quantities.

Figures 2(a) and 2(b) delineate the velocity characteristics as a function of magnetic factor (M) and Weissenberg factor (We). An analogous trend in velocity is discerned for modifications in magnetic factor and Weissenberg factor. The escalation of the magnetic factor decelerates velocity. Magnetic field becomes more formidable with rising magnetic factor. The formidable magnetic field intensifies Lorentz forces and suppresses the fluid flow. The Weissenberg factor characterizes the elastic features of fluids. Higher Weissenberg factor evolves elastic forces and fluid exhibits greater elasticity. Consequently, fluid becomes more resistant to flow and a drop evolves in velocity. The magnetic and Weissenberg factors exert a more pronounced influence on velocity of plane surface than on parabolic surface.

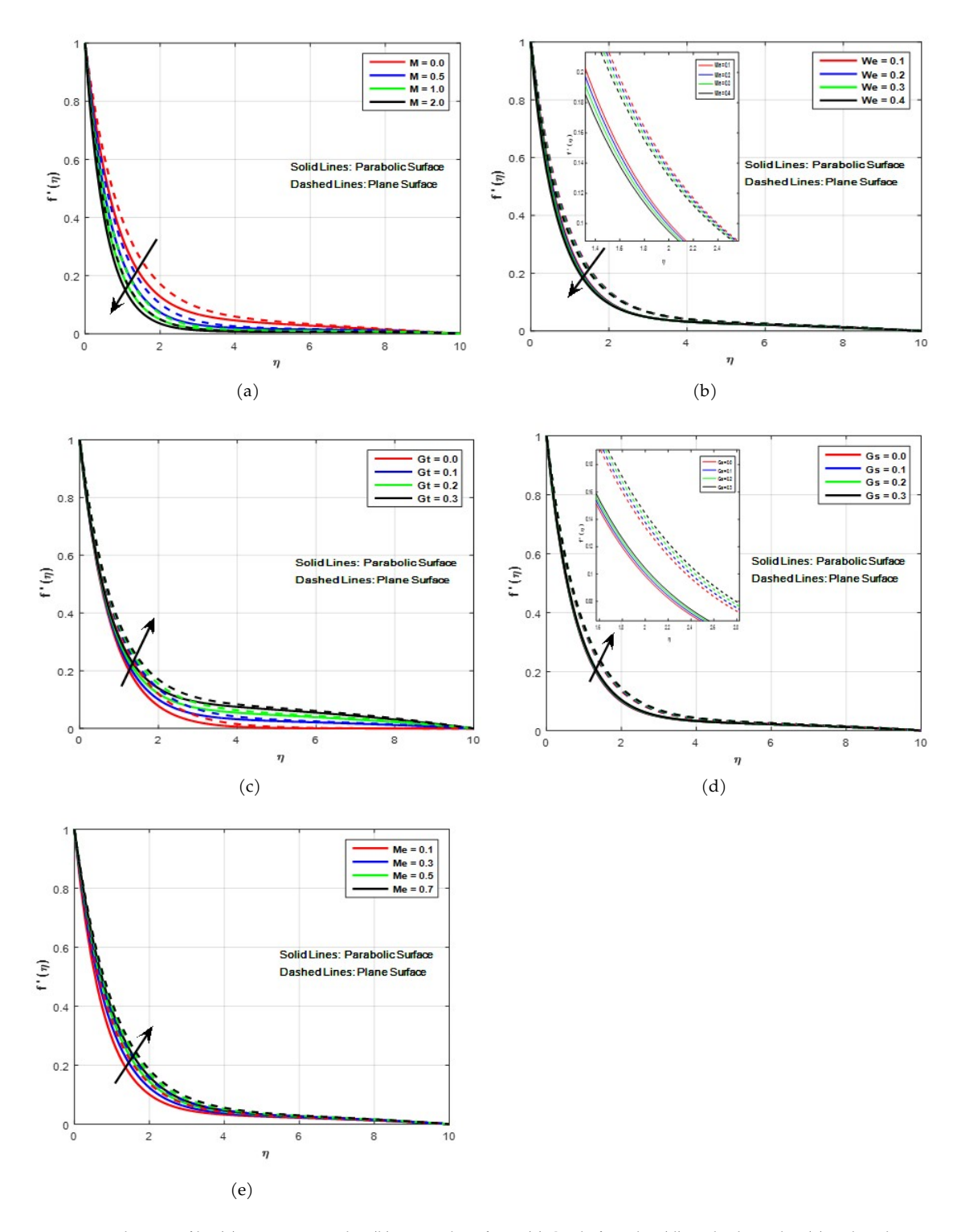
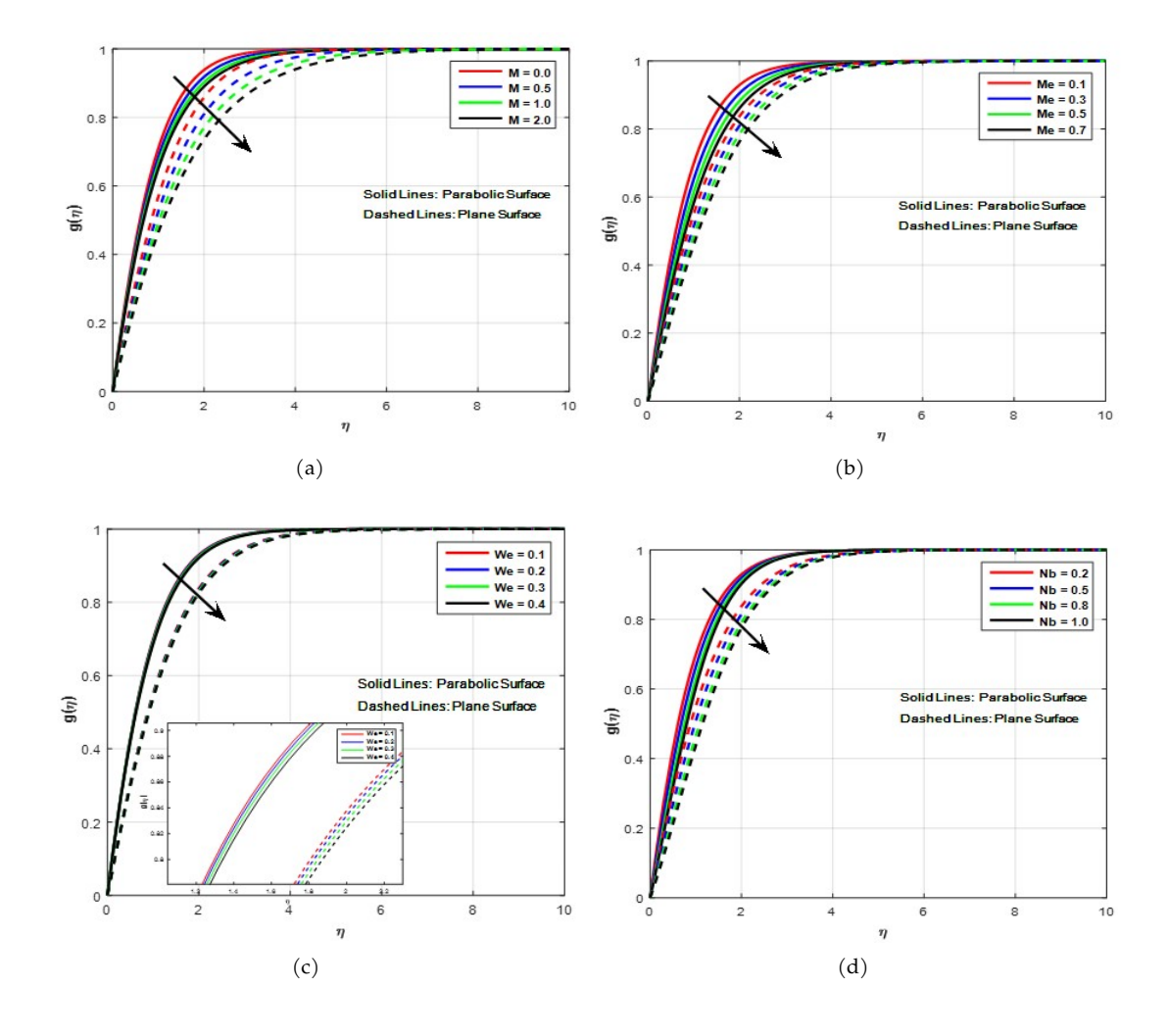


Figure 2: Velocity profiles (a) Hartmann number (b) Weissenberg factor (c) Grashof number (d) Rayleigh number (e) Melting heat.

Figures 2(c)-2(e) showcase velocity patterns influenced by Grashof number (Gt), Rayleigh number (Gs) and melting heat (Me). An escalation in velocity curves is discerned. Typically,

buoyancy force emerges due to thermal discrepancies between adjacent and distant surface areas, enabling us to understand the resulting consequences. Higher Grashof number designates intensified thermal disparities, Facilitating smoother and faster fluid movement and leads to augmentation in velocity. It is evinced in Figure 2(c). A similar pattern is discerned for the Rayleigh number in Figure 2(d). As the Rayleigh number increases, the natural convection becomes more dominant, driving the fluid more vigorously over both parabolic and plane surfaces. The flow geometry of the parabolic surface amplifies this effect, leading to higher velocity compared to the plane surface under similar conditions. This behavior is crucial in understanding and optimizing heat and mass transfer processes in such fluids. The vigorous melting process facilitates intensification in heat transmission from the heated liquid towards the surface, resulting in augmented convective flow and elevated velocity profiles. The increase in velocity with higher melting heat parameter (Me) is due to the reduction in fluid viscosity caused by heat absorption during melting. This enhances the flow near the surface, a trend seen for both parabolic and plane surfaces, with parabolic surfaces maintaining slightly higher velocities due to the effects. It is evinced in Figure 2(e). Compared to plane flow, parabolic flow velocity is more strongly influenced by the aforementioned factors. The melting heat parameter enhances thermal energy and reduces viscous and frictional forces, enabling the fluid to flow more easily and with greater velocity.



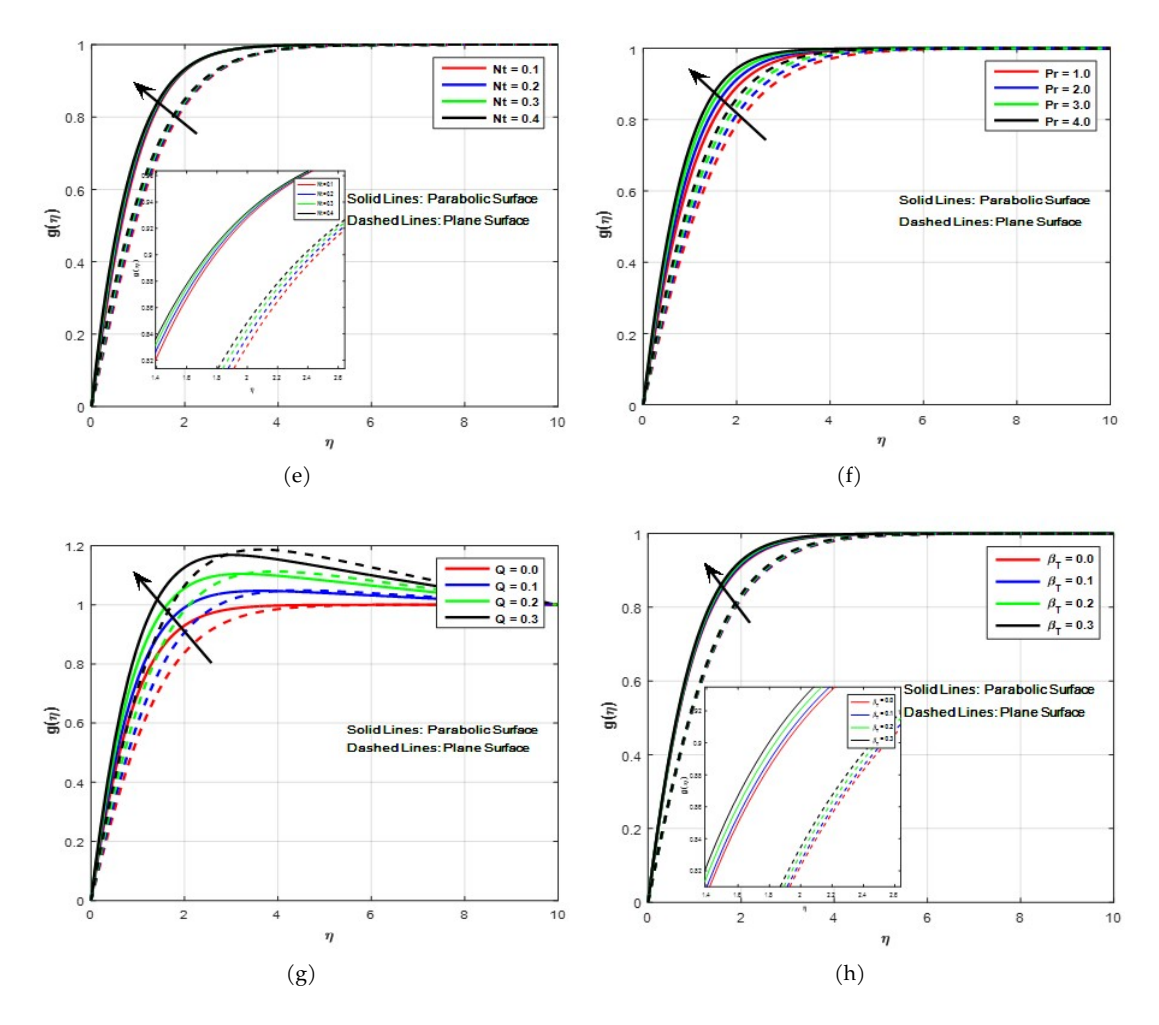
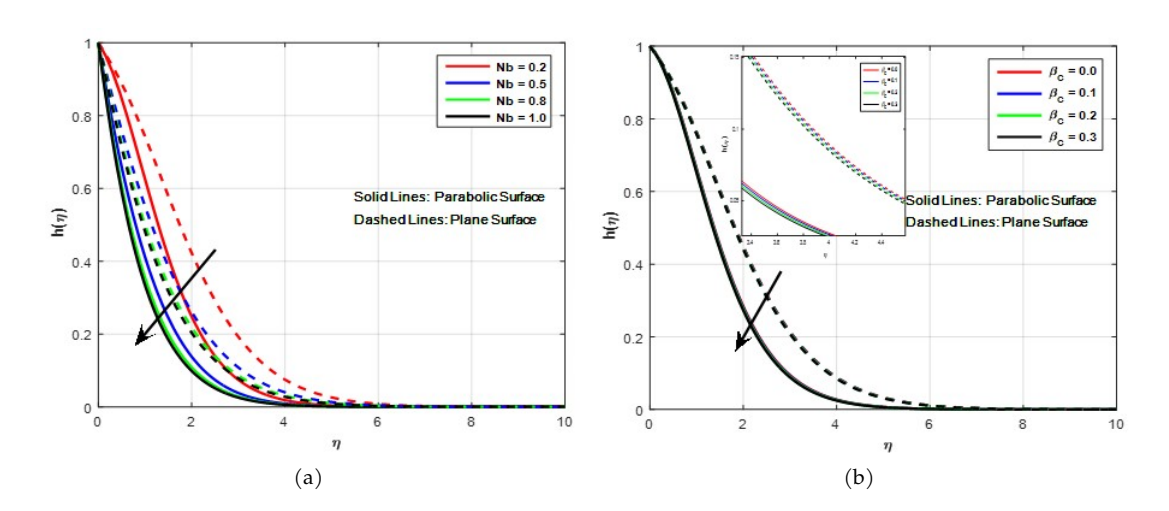


Figure 3: Temperature profiles of (a) Hartmann number (b) Melting heat (c) Weissenberg factor (d) Brownian motion (e) Thermophoretic term (f) Prandtl number (g) Heat source.

Temperature exhibits diminishing nature for enhanced values of magnetic parameter (M), melting factor (Me), Weissenberg factor (We), and for Brownian motion factor (Nb) as shown in Figures 3(a)-3(d). The MHD factor's intensification triggers a temperature drop, as evinced in Figure 3(a). Intensifying the MHD factor typically yields robust magnetic forces. This robust magnetic force and existence of melting heat constraint can inhibit the liquid's heat transmission abilities. Thus, heat flow is obstructed, culminating in a temperature reduction. From Figure 3(b), elevated melting factor estimations lead to downward trend in temperature. Physically, a rise in the melting factor signifies an intensification of heat production due to melting. In reality, the melting process intensifies, enabling greater transfer of heat from the heated liquid to the cold surface and consequently lowering the fluid temperature. As Me increases, the absorption of heat into the melting process reduces the energy available for heating the fluid, leading to lower temperatures. This trend is consistent for both parabolic and plane surfaces, with parabolic surfaces maintaining slightly higher temperatures due to their geometric influence. Increasing the melting heat parameter intensifies heat absorption at the melting interface, leaving less energy to raise the fluid's temperature. Consequently, this leads to a decrease in the fluid's temperature as observed in your study. The drop in temperature as the Weissenberg parameter increases can be attributed to lower viscous dissipation and decreased thermal diffusion. It suppressed convective heat transfer due to the fluid's improved elastic behaviour. As the Brownian motion parameter increases, the amplified random motion of nanoparticles absorbs more thermal energy, reduces the thickness of the thermal boundary layer, and favours mass diffusion over heat diffusion. This energy redistribution causes a decrease in fluid temperature. These effects are observed on parabolic and planar surfaces, as shown in Figures 3(c) and 3(d). Moreover, parabolic flow exhibits a rapid temperature escalation compared to plane flow.

Temperature exhibits escalating trend for enhanced values of thermophoretic term (Nt), Prandtl number (Pr), heat source factor (Q) and thermal relaxation factor ( $\beta_T$ ) as evinced in Figures 3(e)-3(h). Figure 3(e) demonstrates the response of temperature to the elevated thermophoretic factor. Analysis of the figure shows that temperature curves ascend with higher thermophoretic estimations. The proximity of particles to the heated surface induces a thermophoretic force, facilitating particle migration and leading to enhanced thermal conditions. Figure 3(f) sheds light on the complex interaction between and temperature curves. A sharp increase in temperature curves is evinced for Prandtl number's upward shift. The Prandtl number's growth leads to reduced viscous friction. As a result, the predominant portion of energy is utilized for temperature enhancement, bypassing dissipation through viscous friction. With continued Prandtl number escalation, the fluid's heat transmission efficiency amplifies, leading to intensified temperature gradients. The heat source furnishes auxiliary thermal energy, which is then absorbed by the fluid. Heat absorption induces the fluid's temperature to escalate. This phenomenon is visibly demonstrated in Figure 3(g). A similar pattern is discerned for thermal relaxation factor which is delineated in Figure 3(h). The increase in temperature as the thermal relaxation factor increases is due to the delayed heat conduction, enhanced energy storage, and the thickening of the thermal boundary layer. This effect is observed consistently over both parabolic and plane surfaces, as the fluid retains more heat near the surfaces before dissipating it. The interaction of thermal relaxation with viscoelasticity and MHD effects further reinforces this behavior. Moreover, parabolic flow exhibits a rapid temperature escalation compared to plane flow.



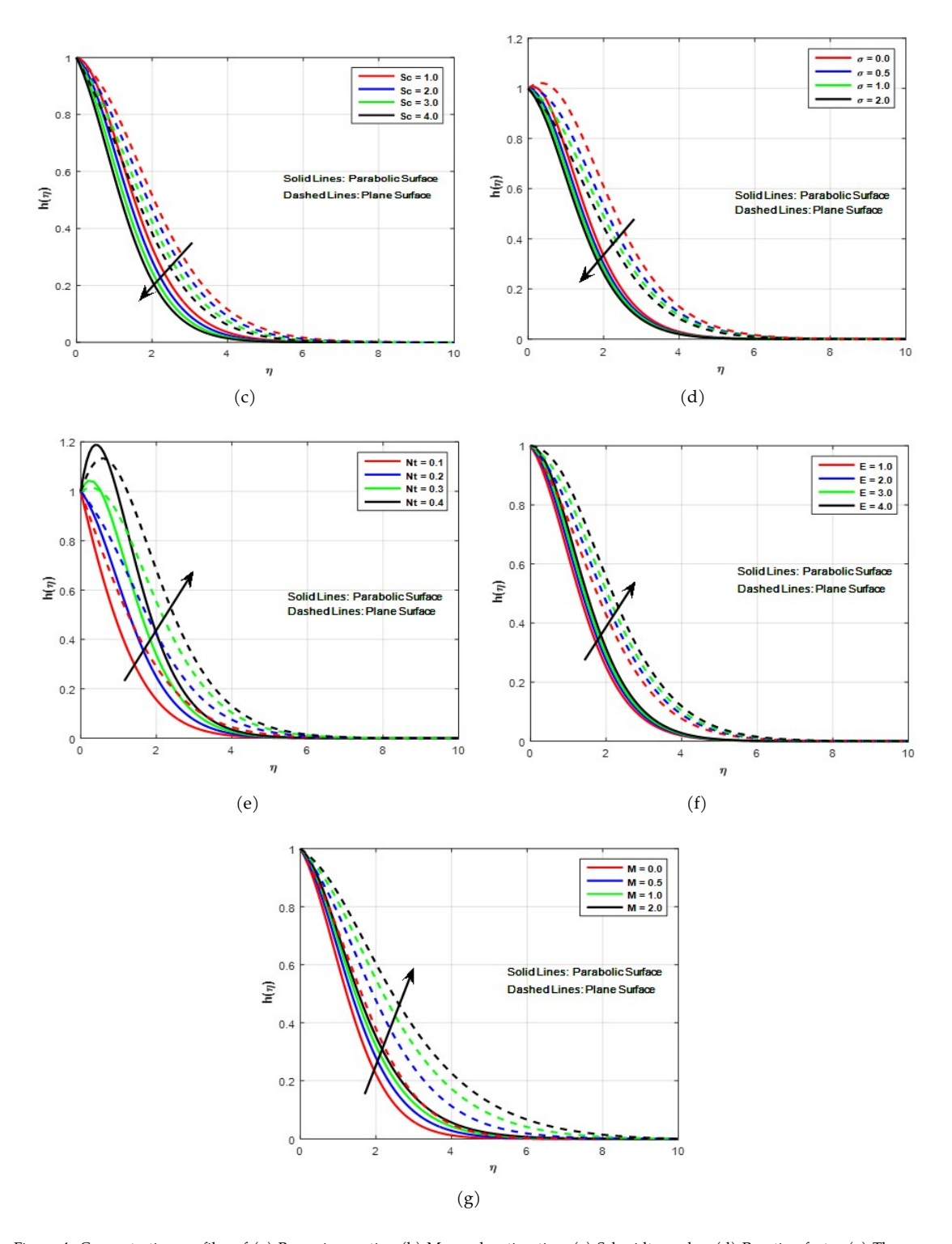


Figure 4: Concentration profiles of (a) Brownian motion (b) Mass relaxation time (c) Schmidt number (d) Reaction factor (e) Thermopherotic term (f) Energy activation number (g) Hartmann number.

Figures 4(a)-4(d) show cases concentration patterns influenced by Brownian motion (Nb), mass relaxation factor  $(\beta_C)$ , Schmidt number (Sc) and reaction factor  $(\sigma)$ . A deceleration in concentration curves is spotted for above factors. Brownian motion significantly affects the concentration of the fluids. Brownian motion induces random particle movements, leading to dispersion and distribution of particles, thereby diminishing concentration gradients that was presented in Figure 4(a). Growing estimations of mass relaxation term drops concentration in Figure 4(b). Intensification in mass relaxation term necessitates longer diffusion times for fluid particles to diffuse. When  $\beta_C = 0$ , diffusion occurs with remarkable speed. From Figure 4(c), it is disclosed that concentration exhibits downward trends for Schmidt number. The reduction in concentration as the Schmidt number (Sc) grows can be attributed to lower mass diffusivity, thinner concentration boundary layers, and momentum's supremacy over mass transfer. Figure 4(d) evinces the impression of influence of reaction parameter  $(\sigma)$  on concentration curves. Concentration curves exhibit substantial decline as the reaction parameter amplifies. Elevating the reaction parameter amplifies the Arrhenius term, ultimately harming the chemical reaction. Thus, the concentration curves exhibit a downward trend. Parabolic flow demonstrates a pronounced concentration drop than in plane flow.

Figures 4(e)-4(g) shows the concentration patterns as a function of thermophoretic term (Nt), energy activation number (E) and magnetic factor (M). From Figure 4(e), amplification of the thermophoretic term triggers a thermophoretic force, directing particles towards colder zones and intensifying diffusion towards these areas, resulting in elevated concentration. From Figure 4(f), amplification of the activation term strengthens concentration gradients. The Arrhenius equation mathematically models activation energy's introduction, illustrating reduced thermal energy and acceleration result in decreased reaction rates, thereby elevating particle concentrations. As E increases, the concentration decreases faster for both surfaces due to higher energy barriers. The geometry influences the rate of decrease, with parabolic surfaces showing slower concentration depletion than plane surfaces. Impression of magnetic factor is evinced in Figure 4(g). A magnetic field interacts with a conducting fluid, generating a Lorentz force that resists fluid motion. This resistance slows down the flow or diffusion of the fluid, preventing the rapid depletion of concentration. Higher M reduces the rate of transport (e.g., diffusion or convection), allowing more molecules or particles to accumulate in the system, resulting in higher concentrations. Parabolic flow demonstrates a pronounced concentration drop than in plane flow.

### 7 Validation

### Nomenclature

(u, v) : Velocity vector (x, y) : Variables

 $T_m, T_{\infty}$ : Sheet temperature, ambient temperature

 $B_0$ : Strength of magnetic field

 $eta_o$  : Volume fraction  $\mu$  : Thermal viscosities  $\nu = \frac{\mu}{o}$  : Kinematic viscosities

*Me* : Melting parameter

 $egin{array}{lll} Q & : & \mbox{Heat source} \\ c_p & : & \mbox{Specific heat} \\ g & : & \mbox{Gravity} \\ \end{array}$ 

 $\eta$  : Similarity variable

Gt: Mixed convection parameter

Gs : Rayleigh number  $\alpha$  : Thickness parameter Pr : Prandtl number Sc : Schmidt number

 $C_W$ : Concentration of the surface  $C_\infty$ : Ambient fluid concentration

E : Energy parameter  $\sigma$  : Reaction parameter

A detailed comparison with previous research is conducted to evaluate the validity of the obtained results and the numerical methods used [1,2]. The drag force is assessed by neutralising (set to zero) other influencing factors and by varying magnetic factor (M), which is evinced in Table 1. The congruent results provide robust confirmation of the coding approach. So, an in-depth analysis of recent scholarly work confirms that the advocated numerical technique and accompanying results are exceedingly reliable and dependable. The table presents a comparative study of the values computed for a specific parameter M using three different methods: the reports by Akbar et al. [4], Malik et al. [39], and the bvp4c method. Across the range of M values, the results from all three methods are closely aligned, showing minimal variation. For smaller M values, such as 0, 0.5, and 1, the differences are negligible, highlighting the high accuracy of all approaches. However, as M increases, the slight differences become more apparent due to the precision limits of the methods. For example, at M=1000, the values are very close but not identical: This comparison demonstrates that while all methods provide consistent and reliable results, bvp4c offers higher precision due to its advanced computational capabilities.

Table 1: Comparative study of -f''(0) with the existing reports for m=1 in the absence of other parameters.

$\overline{M}$	Akbar et al. [4]	Malik et al. [39]	bvp4c
0	1.0000	1.0000	10000747
0.5	1.11803	1.11802	1.11803448
1	1.41421	1.41419	1.41421356
5	2.44949	2.44945	2.44948974
10	3.31663	3.31657	3.31662479
100	10.04988	10.04981	10.04987518
500	22.38303	22.38294	22.38302912
1000	31.63859	31.63851	31.63858418

Table 2 illustrates the influence of parameter variations on surface drag for parabolic and plane configurations. As We increase, the skin friction increases for parabolic and plane surfaces, with parabolic surfaces consistently showing higher values. This indicates that viscoelastic effects enhance resistance to flow, with geometry playing a significant role. Skin friction increases with M, showing the magnetic field's suppressive effect (Lorentz force) on the velocity. Parabolic surfaces exhibit greater skin friction than plane surfaces, likely due to curvature amplifying the magnetic damping effect. Increasing Gt (positive values correspond to aiding flow) reduces skin friction, as buoyancy assists fluid movement, lowering resistance. Both surfaces show this trend, but the parabolic surface retains higher skin friction. Increasing Gs decreases skin friction on both surfaces, reflecting the dominance of thermal buoyancy forces in reducing viscous resistance.

Parabolic surfaces exhibit a more significant decline compared to plane surfaces. As the Melting parameter increases, skin friction decreases on both surfaces, indicating that melting at the interface absorbs energy and reduces the boundary layer's resistance. Again, parabolic surfaces maintain higher skin friction compared to plane surfaces.

We	M	$G_t$	Gs	Me	Parabolic surface	Plane surface
0.1					1.27314982	1.09073852
0.2					1.34923427	1.13775836
0.3					1.45740724	1.19844473
	0.0				1.15534306	0.98234129
	0.5				1.42836365	1.23637813
	1.0				1.65272684	1.45003968
		0.2			1.25635615	1.08161140
		0.5			1.17178975	1.03417596
		0.8			1.21150823	1.05673623
			0.2		1.26483493	1.08279900
			0.5		1.24026787	1.05948487
			0.8		1.21622189	1.03682667
				0.2	1.22691370	1.06641822
				0.4	1.15426219	1.02650051
				0.6	1.09903896	0.99479613

Table 2: A comparative study of skin friction.

Table 3 illustrates the influence of parameter variations on Nusselt number for parabolic and plane configurations. The Nusselt number decreases slightly for both surfaces as We increase, indicating reduced heat transfer efficiency due to the fluid's visco elasticity. The decrease is more pronounced for the plane surface. As M increases, the Nusselt number decreases for both surfaces, showing that the magnetic field dampens the flow and thermal gradients, leading to lower heat transfer. The reduction is more significant for the plane surface. Higher Gt and Gs values generally enhance the Nusselt number on both surfaces, emphasising the role of buoyancy in promoting convective heat transfer. Parabolic surfaces experience a more substantial increase due to their geometry. As Me increases, the Nusselt number rises for both surfaces. This indicates that the enhanced melting process improves heat transfer by thinning the thermal boundary layer. Due to their curved geometry, parabolic surfaces show a consistently higher Nusselt number than plane surfaces.

Table 4 illustrates the influence of parameter variations on Sherwood number for parabolic and plane configurations. As We increases, the Sherwood number decreases for both surfaces, indicating that viscoelastic effects reduce the mass transfer rate. Plane surfaces exhibit slightly higher Sherwood numbers than parabolic surfaces. Increasing M decreases the Sherwood number, as the Lorentz force slows fluid motion, reducing the mass transfer rate. This trend is observed for both surfaces, with plane surfaces showing marginally higher values. As Gc increases, the Sherwood number rises, reflecting enhanced mass transfer due to buoyancy effects aiding diffusion. Plane surfaces again show slightly higher values. As E increases, the Sherwood number increases for both surfaces, suggesting that higher energy levels enhance species diffusion. Plane surfaces maintain higher mass transfer rates compared to parabolic ones. Increasing  $\sigma$  (representing reaction strength) decreases the Sherwood number, as stronger chemical reactions consume diffusing

species, reducing the mass transfer rate. The plane surface exhibits higher values across the range.

From Tables 2, 3, and 4, it is evinced that the parabolic surface demonstrates superior skin friction and heat transmission accompanied by reduced mass transport compared to plane surfaces.

Table 3: A comparative study of Nusselt number.

We	M	$G_t$	Me	Q	$\beta_t$	Parabolic surface	Plane surface
0.1						1.01823044	0.64130867
0.2						1.01240333	0.63644202
0.3						1.00547127	0.63092658
	0.0					1.03535468	0.66409567
	0.5					0.99690030	0.61188697
	1.0					0.96845241	0.57146113
		0.2				1.02350308	0.64696301
		0.5				1.03658393	0.66072385
		0.8				1.04721698	0.67174158
			0.2			0.94429912	0.60335688
			0.4			0.83012205	0.54176285
			0.6			0.74479818	0.49350644
				0.1		1.10180702	0.70633667
				0.2		1.19384871	0.77961589
				0.3		1.29550198	0.86254529
					0.1	0.99451191	0.63201865
					0.2	0.99708662	0.63303449
					0.3	0.99967619	0.63405439

Table 4: A comparative study of Shearwood number.

We	M	Gc	$\sigma$	E	Parabolic surface	Plane Surface
0.1					0.19514845	0.20038384
0.2					0.18936130	0.19683424
0.3					0.18290788	0.19300631
	0.0				0.22207607	0.22777591
	0.5				0.16396831	0.16742554
	1.0				0.12660306	0.12733443
		0.2			0.19722529	0.20302409
		0.5			0.20320935	0.21036039
		0.8			0.20886234	0.21698213
			0.1		0.07742346	0.08625472
			0.5		0.14980188	0.15760089
			1.0		0.14980188	0.15760089
				2	0.20335758	0.20784054
				3	0.18681034	0.19276829
				4	0.16537019	0.17298420

### 8 Conclusion

A novel comparative scrutiny is carried out on parabolic and plane surfaces in the context of Williamson fluid. This study delineates the complex interactions among several critical factors like activation energy and melting heat accounting for supplementary factors such as mixed convection, heat source. This research endeavors to impart insight into the multifaceted relationships between various factors affecting fluid flow and elucidate the underlying mechanisms that influence the flow dynamics. The prime conclusions are:

- The magnetic and Weissenberg factors exert a more pronounced influence on velocity of plane surface than on parabolic surface.
- Compared to plane flow, parabolic flow velocity is more strongly influenced by the melting factor.
- Parabolic flow exhibits a rapid temperature escalation compared to plane flow.
- Parabolic flow demonstrates a pronounced concentration drop than in plane flow.
- Elevated melting factor estimations lead to downward trend in temperature and elevation in velocity.
- Heat source and thermal relaxation factors induces escalation in the fluid's temperature.
- Concentration curves exhibit substantial decline for reaction parameter and mass relaxation factors.
- Amplification of the activation term strengthens concentration gradients.

**Acknowledgement** The authors sincerely thank the editor for their invaluable guidance and support throughout the review process. We are deeply grateful to the anonymous reviewers for their constructive comments and insightful suggestions, which have significantly enhanced the quality of this manuscript.

**Conflicts of Interest** The authors declare no conflict of interest.

### References

- [1] O. A. Abegunrin, I. L. Animasaun & N. Sandeep (2018). Insight into the boundary layer flow of non–Newtonian Eyring–Powell fluid due to catalytic surface reaction on an upper horizontal surface of a paraboloid of revolution. *Alexandria Engineering Journal*, 57(3), 2051–2060. https://doi.org/10.1016/j.aej.2017.05.018.
- [2] O. A. Abegunrin, S. O. Okhuevbie & I. L. Animasaun (2016). Comparison between the flow of two non–Newtonian fluids over an upper horizontal surface of paraboloid of revolution: Boundary layer analysis. *Alexandria Engineering Journal*, 55(3), 1915–1929. https://doi.org/10.1016/j.aej.2016.08.002.
- [3] O. A. Abegunrin & I. L. Animasaun (2017). Motion of Williamson fluid over an upper horizontal surface of a paraboloid of revolution due to partial slip and buoyancy: Boundary layer

- analysis. *Transfer Phenomena in Fluid and Heat Flows IV*, 378, 16–27. https://doi.org/10.4028/www.scientific.net/DDF.378.16.
- [4] N. S. Akbar, A. Ebaid & Z. H. Khan (2015). Numerical analysis of magnetic field effects on Eyring–Powell fluid flow towards a stretching sheet. *Journal of Magnetism and Magnetic Materials*, 382, 355–358. https://doi.org/10.1016/j.jmmm.2015.01.088.
- [5] A. Ali, M. Hussain, M. S. Anwar & M. Inc (2021). Mathematical modeling and parametric investigation of blood flow through a stenosis artery. *Applied Mathematics and Mechanics*, 42, 1675–1684. https://doi.org/10.1007/s10483-021-2791-8.
- [6] F. E. Alsaadi, I. Ullah, T. Hayat & F. E. Alsaadi (2020). Entropy generation in nonlinear mixed convective flow of nanofluid in porous space influenced by Arrhenius activation energy and thermal radiation. *Journal of Thermal Analysis and Calorimetry*, 140, 799–809. https://doi.org/ 10.1007/s10973-019-08648-0.
- [7] K. Alsa'di, N. M. A. Nik Long & Z. K. Eshkuvatov (2024). Theoretical and numerical studies of fractional Volterra–Fredholm integro-differential equations in Banach space. *Malaysian Journal of Mathematical Sciences*, 18(3), 469–489. https://doi.org/10.47836/mjms.18.3.01.
- [8] I. L. Animasaun, B. Mahanthesh, G. Sarojamma & J. S. Damisa (2020). Significance of thickness of paraboloid of revolution and buoyancy forces on the dynamics of Erying–Powell fluid subject to equal diffusivity kind of quartic autocatalysis. *Physica A: Statistical Mechanics and its Applications*, 549, Article ID: 124047. https://doi.org/10.1016/j.physa.2019.124047.
- [9] I. L. Animasaun & N. Sandeep (2016). Buoyancy induced model for the flow of 36 nm alumina-water nanofluid along upper horizontal surface of a paraboloid of revolution with variable thermal conductivity and viscosity. *Powder Technology*, 301, 858–867. https://doi.org/10.1016/j.powtec.2016.07.023.
- [10] M. S. Anwar, M. Khan, Z. Hussain, T. Muhammad & V. Puneeth (2025). Investigation of heat transfer characteristics in MHD hybrid nanofluids with variable viscosity and thermal radiations. *Journal of Radiation Research and Applied Sciences*, 18(1), Article ID: 101240. https: //doi.org/10.1016/j.jrras.2024.101240.
- [11] M. S. Anwar, M. S. Alqarni & M. Irfan (2024). Exploring the marvels of heat transfer: MHD convection at a stagnation point in non–Newtonian fluid with yield stress and chemical reactions. *Chinese Journal of Physics*, 89, 1299–1308. https://doi.org/10.1016/j.cjph.2024.01.030.
- [12] E. Azhar, E. N. Maraj, H. Afaq, M. Jamal & Z. Iqbal (2024). Application of activation energy and Joule heating with variable viscosity on MHD flow of trihybrid nanofluid over a disk. *International Communications in Heat and Mass Transfer*, 155, Article ID: 107573. https://doi.org/10.1016/j.icheatmasstransfer.2024.107573.
- [13] W. F. W. Azmi, A. Q. Mohamad, L. Y. Jiann & S. Shafie (2024). Mathematical fractional analysis on blood Casson fluid in slip and small arteries with the cholesterol porosity effect. *Malaysian Journal of Mathematical Sciences*, 18(4), 755–774. https://doi.org/10.47836/mjms. 18.4.05.
- [14] A. R. Bestman (1990). Natural convection boundary layer with suction and mass transfer in a porous medium. *International Journal of Energy Research*, 14(4), 389–396. https://doi.org/10.1002/er.4440140403.
- [15] C. Cattaneo (2011). Some Aspects of Diffusion Theory, volume 42 of C.I.M.E. Summer Schools, chapter Sulla Conduzione Del Calore, pp. 485. Springer, Berlin, Heidelberg. https://doi.org/ 10.1007/978-3-642-11051-1\_5.

- [16] M. S. Dada & C. Onwubuoya (2020). Variable viscosity and thermal conductivity effects on Williamson fluid flow over a slendering stretching sheet. *World Journal of Engineering*, 17(3), 357–371. http://dx.doi.org/10.1108/WJE-08-2019-0222.
- [17] R. T. Davis & M. J. Werle (1972). Numerical solutions for laminar incompressible flow past a paraboloid of revolution. *AIAA Journal*, 10(9), 224–230. https://doi.org/10.2514/3.50354.
- [18] M. P. Devi & S. Srinivas (2023). Heat transfer effects on the oscillatory MHD flow in a porous channel with two immiscible fluids. *Nonlinear Analysis: Modelling and Control*, 28(3), 393–411. https://doi.org/10.15388/namc.2023.28.31503.
- [19] B. S. Dhruvathara, K. G. Kumar, W. Sharaf Saeed & A. Afzal (2023). EMHD flow and convective heat transfer over a prescribed surface temperature (PST) and prescribed heat flux (PHF) heating condition. *Numerical Heat Transfer, Part A: Applications*, 86(2), 201–214. https://doi.org/10.1080/10407782.2023.2261144.
- [20] J. B. J. Fourier (1888). *Théorie Analytique de La Chaleur* volume 1. Gauthier-Villars, New Brunswick.
- [21] K. Ganesh Kumar, A. Baslem, B. C. Prasannakumara, J. Majdoubi, M. Rahimi-Gorji & S. Nadeem (2020). Significance of Arrhenius activation energy in flow and heat transfer of tangent hyperbolic fluid with zero mass flux condition. *Microsystem Technologies*, 26, 2517–2526. https://doi.org/10.1007/s00542-020-04792-y.
- [22] K. Ganesh Kumar, D. G. Prakasha, M. M. Praveen, M. Gnaneswara Reddy & K. R. Vasanth (2024). Physical characteristics of variable thermal conductivity and MHD flow across a continually stretched sheet. *Proceedings of the Institution of Mechanical Engineers, Part N: Journal of Nanomaterials, Nanoengineering and Nanosystems*, pp. Article ID: 23977914241259087. https://doi.org/10.1177/23977914241259087.
- [23] K. Gangadhar, P. Manasa Seshakumari, M. Venkata Subba Rao & A. J. Chamkha (2022). Biconvective transport of magnetized couple stress fluid over a radiative paraboloid of revolution. *Proceedings of the Institution of Mechanical Engineers, Part E: Journal of Process Mechanical Engineering*, 236(4), 1661–1670. https://doi.org/10.1177/09544089211072715.
- [24] T. Hayat, S. Ayub, A. Tanveer & A. Alsaedi (2018). Numerical simulation for MHD Williamson fluid utilizing modified Darcy's law. *Results in Physics*, 10, 751–759. https://doi.org/10.1016/j.rinp.2018.06.055.
- [25] J. Hron, J. Málek, P. Pustějovská & K. R. Rajagopal (2010). On the modeling of the synovial fluid. *Advances in Tribology*, 2010(1), Article ID: 104957. https://doi.org/10.1155/2010/104957.
- [26] Z. Hussain, T. Hayat, A. Alsaedi & M. S. Anwar (2021). Mixed convective flow of CNTs nanofluid subject to varying viscosity and reactions. *Scientific Reports*, 11(1), Article ID: 22838. https://doi.org/10.1038/s41598-021-02228-9.
- [27] M. Irfan, W. A. Khan, M. Khan & M. M. Gulzar (2019). Influence of Arrhenius activation energy in chemically reactive radiative flow of 3D Carreau nanofluid with nonlinear mixed convection. *Journal of Physics and Chemistry of Solids*, 125, 141–152. https://doi.org/10.1016/j.jpcs.2018.10.016.
- [28] M. Irfan, P. Sunthrayuth, A. Ali Pasha, M. S. Anwar & W. Azeem Khan (2025). Phenomena of thermo-sloutal time's relaxation in mixed convection Carreau fluid with heat sink/source. *Waves in Random and Complex Media*, 35(2), 4008–4020. https://doi.org/10.1080/17455030. 2022.2056658.

- [29] K. A. Khan, M. F. Javed, M. A. Ullah & M. B. Riaz (2023). Heat and mass transport analysis for Williamson MHD nanofluid flow over a stretched sheet. *Results in Physics*, *53*, Article ID: 106873. https://doi.org/10.1016/j.rinp.2023.106873.
- [30] M. Khan, M. Y. Malik, T. Salahuddin & A. Hussian (2018). Heat and mass transfer of Williamson nanofluid flow yield by an inclined Lorentz force over a nonlinear stretching sheet. *Results in Physics*, *8*, 862–868. https://doi.org/10.1016/j.rinp.2018.01.005.
- [31] M. Khan, A. Rasheed & M. S. Anwar (2023). Numerical analysis of nonlinear time-fractional fluid models for simulating heat transport processes in porous medium. *ZAMM-Journal of Applied Mathematics and Mechanics/Zeitschrift für Angewandte Mathematik und Mechanik*, 103(9), Article ID: e202200544. https://doi.org/10.1002/zamm.202200544.
- [32] N. S. Khan, S. Akhter, I. Kebaili, F. M. O. Birkea & R. H. Egami (2024). Dynamic processes of quartic autocatalysis chemical reaction in Williamson nanofluid flow over a parabolic surface. *Thermal Science and Engineering Progress*, *54*, Article ID: 102798. https://doi.org/10.1016/j.tsep.2024.102798.
- [33] Y. B. Kho, A. Hussanan, M. K. A. Mohamed & M. Z. Salleh (2019). Heat and mass transfer analysis on flow of Williamson nanofluid with thermal and velocity slips: Buongiorno model. *Propulsion and Power Research*, 8(3), 243–252. https://doi.org/10.1016/j.jppr.2019.01.011.
- [34] O. K. Koriko, A. J. Omowaye, N. Sandeep & I. L. Animasaun (2017). Analysis of boundary layer formed on an upper horizontal surface of a paraboloid of revolution within nanofluid flow in the presence of thermophoresis and brownian motion of 29 nm CuO. *International Journal of Mechanical Sciences*, 124, 22–36. https://doi.org/10.1016/j.ijmecsci.2017.02.020.
- [35] G. Kumaran & N. Sandeep (2017). Thermophoresis and Brownian moment effects on parabolic flow of MHD Casson and Williamson fluids with cross diffusion. *Journal of Molecular Liquids*, 233, 262–269. https://doi.org/10.1016/j.molliq.2017.03.031.
- [36] F. Loix, L. Orgéas, C. Geindreau, P. Badel, P. Boisse & J. F. Bloch (2009). Flow of non–Newtonian liquid polymers through deformed composites reinforcements. *Composites Science and Technology*, 69(5), 612–619. https://doi.org/10.1016/j.compscitech.2008.12.007.
- [37] O. D. Makinde & I. L. Animasaun (2016). Bioconvection in MHD nanofluid flow with nonlinear thermal radiation and quartic autocatalysis chemical reaction past an upper surface of a paraboloid of revolution. *International Journal of Thermal Sciences*, 109, 159–171. https://doi.org/10.1016/j.ijthermalsci.2016.06.003.
- [38] O. D. Makinde, P. O. Olanrewaju & W. M. Charles (2011). Unsteady convection with chemical reaction and radiative heat transfer past a flat porous plate moving through a binary mixture. *Afrika Matematika*, 22, 65–78. https://doi.org/10.1007/s13370-011-0008-z.
- [39] M. Y. Malik, T. Salahuddin, A. Hussain & S. Bilal (2015). MHD flow of tangent hyperbolic fluid over a stretching cylinder: Using Keller box method. *Journal of Magnetism and Magnetic Materials*, 395, 271–276. https://doi.org/10.1016/j.jmmm.2015.07.097.
- [40] M. Mustafa (2015). Cattaneo–Christov heat flux model for rotating flow and heat transfer of upper-convected Maxwell fluid. *AIP Advances*, 5(4), Article ID: 047109. https://doi.org/10.1063/1.4917306.
- [41] S. Nadeem, S. T. Hussain & C. Lee (2013). Flow of a Williamson fluid over a stretching sheet. *Brazilian Journal of Chemical Engineering*, 30, 619–625. https://doi.org/10.1590/S0104-66322013000300019.

- [42] L. S. Naik, D. G. Prakasha, M. V. V. N. L. Sudharani & K. Ganesh Kumar (2024). Effects of ohmic and activation energy on the physical characteristics of MHD flow and variable heat transfer to a different fluids. *International Journal of Modern Physics B*, 38(18), Article ID: 2450241. https://doi.org/10.1142/S0217979224502412.
- [43] K. M. Nihaal, U. S. Mahabaleshwar & S. W. Joo (2024). Darcy Forchhiemer imposed exponential heat source-sink and activation energy with the effects of bioconvection over radially stretching disc. *Scientific Reports*, 14(1), Article ID: 7910. https://doi.org/10.1038/s41598-024-58051-5.
- [44] M. Padma Devi, S. Srinivas & K. Vajravelu (2024). Entropy generation in two-immiscible MHD flow of pulsating Casson fluid in a vertical porous space with Slip effects. *Journal of Thermal Analysis and Calorimetry*, 149(14), 7449–7468. https://doi.org/10.1007/s10973-024-13337-8.
- [45] A. Rasheed & M. S. Anwar (2018). Numerical computations of fractional nonlinear Hartmann flow with revised heat flux model. *Computers & Mathematics with Applications*, 76(10), 2421–2433. https://doi.org/10.1016/j.camwa.2018.08.039.
- [46] Y. D. Reddy, F. Mebarek-Oudina, B. S. Goud & A. I. Ismail (2022). Radiation, velocity and thermal slips effect toward MHD boundary layer flow through heat and mass transport of Williamson nanofluid with porous medium. *Arabian Journal for Science and Engineering*, 47(12), 16355–16369. https://doi.org/10.1007/s13369-022-06825-2.
- [47] J. A. Rojas & K. Santos (2013). Magnetic nanophases of iron oxide embedded in polymer. Effects of magneto-hydrodynamic treatment of pure and wastewater. In *V Latin American Congress on Biomedical Engineering CLAIB 2011 May 16-21, 2011, Habana, Cuba,* volume 33 of *IFMBE Proceedings* pp. 37–40. Springer, Berlin Heidelberg. https://doi.org/10. 1007/978-3-642-21198-0\_10.
- [48] T. Salahuddin, M. Y. Malik, A. Hussain, S. Bilal & M. Awais (2016). MHD flow of Cattanneo–Christov heat flux model for Williamson fluid over a stretching sheet with variable thickness: Using numerical approach. *Journal of Magnetism and Magnetic Materials*, 401, 991–997. https://doi.org/10.1016/j.jmmm.2015.11.022.
- [49] P. N. Santoshi, G. V. R. Reddy & P. Padma (2020). Flow features of non-newtonian fluid through a paraboloid of revolution. *International Journal of Applied and Computational Mathematics*, 6, 1–22. https://doi.org/10.1007/s40819-020-00828-z.
- [50] A. Shafiq & T. N. Sindhu (2017). Statistical study of hydromagnetic boundary layer flow of Williamson fluid regarding a radiative surface. *Results in Physics*, 7, 3059–3067. https://doi.org/10.1016/j.rinp.2017.07.077.
- [51] Z. Shah, E. Bonyah, S. Islam, W. Khan & M. Ishaq (2018). Radiative MHD thin film flow of Williamson fluid over an unsteady permeable stretching sheet. *Heliyon*, 4(10), Article ID: e00825. https://doi.org/10.1016/j.heliyon.2018.e00825.
- [52] N. S. Shashikumar, M. Madhu, S. Sindhu, B. J. Gireesha & N. Kishan (2021). Thermal analysis of MHD Williamson fluid flow through a microchannel. *International Communications in Heat and Mass Transfer*, 127, Article ID: 105582. https://doi.org/10.1016/j.icheatmasstransfer.2021. 105582.
- [53] H. M. Shawky, N. T. M. Eldabe, K. A. Kamel & E. A. Abd-Aziz (2019). MHD flow with heat and mass transfer of Williamson nanofluid over stretching sheet through porous medium. *Microsystem Technologies*, 25, 1155–1169. https://doi.org/10.1007/s00542-018-4081-1.

- [54] L. Sing Naik, D. G. Prakasha, M. V. V. N. L. Sudharani & K. Ganesh Kumar (2024). A bidirectional investigation of the effect of activation energy on carbonized fluid flow and radiative heat transfer across a stretched surface. *International Journal of Modern Physics B*, 38(09), Article ID: 2450134. https://doi.org/10.1142/S0217979224501340.
- [55] P. R. Sobhana Babu, P. Jayalakshmi, D. V. N. S. R. Murthy, C. Srinivasulu & W. Sridhar (2024). Numerical investigation of Williamson fluid in presence of chemical reaction towards a parabolic surface. *International Journal of Modelling and Simulation*, pp. 1–13. https://doi.org/10.1080/02286203.2024.2441487.
- [56] T. Srinivasulu & B. S. Goud (2021). Effect of inclined magnetic field on flow, heat and mass transfer of Williamson nanofluid over a stretching sheet. *Case Studies in Thermal Engineering*, 23, Article ID: 100819. https://doi.org/10.1016/j.csite.2020.100819.
- [57] H. Yamaguchi, X. R. Zhang, S. Higashi & M. Li (2008). Study on power generation using electro-conductive polymer and its mixture with magnetic fluid. *Journal of Magnetism and Magnetic Materials*, 320(7), 1406–1411. https://doi.org/10.1016/j.jmmm.2007.12.014.
- [58] A. Zeeshan, Z. Ali, M. R. Gorji, F. Hussain & S. Nadeem (2020). Flow analysis of biconvective heat and mass transfer of two-dimensional couple stress fluid over a paraboloid of revolution. *International Journal of Modern Physics B*, 34(11), Article ID: 2050110. https://doi.org/10.1142/S0217979220501106.